Flexible terahertz wire grid polarizer with high extinction ratio and low loss

Article (Accepted Version)

Flexible terahertz wire grid polarizer with high extinction ratio and low loss

A. Ferraro[1,2,*], D. C. Zografopoulos[1], M. Missori[3], M. Peccianti[3,4], R. Caputo[2], and R. Beccherelli[1]

[1]Consiglio Nazionale delle Ricerche, Istituto per la Microelettronica e Microsistemi (CNR-IMM), Roma 00133, Italy
[2]Department of Physics and CNR-NANOTEC, University of Calabria, I-87036 Rende (CS), Italy
[3]Consiglio Nazionale delle Ricerche, Istituto dei Sistemi Complessi (CNR-ISC), Roma 00185, Italy
[4]Department of Physics and Astronomy, University of Sussex, Falmer, Brighton BN1 9RH, United Kingdom
[*]Corresponding author: antonio.ferraro@artov.imm.cnr.it

Compiled March 31, 2016

An aluminum-based THz wire grid polarizer is theoretically investigated and experimentally demonstrated on a sub-wavelength thin flexible and conformal foil of the cyclo-olefin Zeonor© polymer. THz time-domain spectroscopy characterization, performed on both flat and curved configurations, reveals a high extinction ratio between 40 and 45 dB in the 0.3-1 THz range and in excess of 30 dB up to 2.5 THz. The insertion losses are lower than 1 dB and are almost exclusively due to moderate Fabry-Perót reflections, which vanish at targeted frequencies. The polarizer can be easily fabricated with low-cost techniques such as roll-to-roll and/or large-area electronics processes and promises to open the way for a new class of flexible and conformal THz devices.

OCIS codes: *230.5440, 310.5448, 220.4000, 300.6495, 050.6624*

http://dx.doi.org/10.1364/OL.30.XXXXXX

In recent years, terahertz (THz) frequencies have attracted much scientific attention in order to fill the THz-gap between microwaves and optical frequencies in the electromagnetic spectrum. The rationale of this trend is to be found in the numerous applications of THz radiation in cross-disciplinary fields, such as secure short-range communications [1, 2], defense and security [3], explosive and drug detection [4], or life-science [5]. In this context, there is a sharp demand of THz components with functionality equivalent to those used in optics, *e.g.* beam splitters [6], phase shifters [7, 8], and absorbers [9, 10].

Analyzing and controlling the polarization of waves is a key basic function in applications dealing with electromagnetic propagation in any part of the spectrum, including the THz band [11]. In general, the particular feature that characterizes THz sources such as quantum cascade lasers [12], diode based frequency multipliers [13], vacuum tubes (BWO, Gyratron, FEL, etc.) [14] is that their output radiation is only partially polarized. Conversely, terahertz time domain spectroscopy (TDS) setups often employ a photoconductive antenna emitter, which inherently exhibits a polarized emission. It is worth noting that, although in optics prism polarizers offer 50-60 dB extinction ratio (ER) and low insertion losses (IL) and polymer-based dichroic polarizers offer 30-40 dB at a negligible cost, no equivalent devices exist at THz mainly due to material absorption.

Various THz polarizers have been so far developed using different approaches, for instance based on aligned carbon nanotubes [15], nematic liquid crystals [16], tunable metamaterials [17], thin film metallic gratings [18, 19], or spoof surface plasmon polaritons [20]. Among them, the most popular approach is based on wire grids, either freestanding or deposited on a dielectric substrate. In most respects, a wire grid polarizer (WGP) with a deep sub-wavelength pitch can be thought of as the simplest metamaterial device. Its anisotropic performance stems from the inherent polarization-dependent nature of the induced currents in the metal. Readily available freestanding THz WGP offer high transmittance [21]. However, they are expensive to make and mechanically fragile. Conversely, wire-grid patterns on a dielectric substrate are less expensive and easier to produce, because they can be fabricated using standard photolithography, as well as various large-area techniques. In [22] an ER of 35 dB at 0.5 THz is achieved, but the transmittance of the polarizer is approximately 50% owing to the high reflectivity of the Si substrate. In [23] Pickwell-MacPherson's group achieved an ER between 20 and 49 dB in the 0.2-2 THz range and an IL lower than 1 dB. Nevertheless, the employed fabrication process relies on dry bulk micromachining of a silicon wafer. As such, it requires a significant amount of process consumables. Although a wet-etch process may reduce the cost, the silicon based process is intrinsically constrained by the size of crystalline wafer. A technique to improve the ER performance of the WGP is to fabricate a bilayer [24] or multilayer structure [25]. In both cases two or more single WGP are stacked together, therefore increasing the number of fabrication steps and hence the overall complexity and cost. Takano *et al.* [26] have fabricated a WGP on a flexible substrate with 140 nm pitch by means nano-imprinting, but the device shows significant losses.

In this work, we experimentally demonstrate an Al-based THz WGP with very low IL and high ER fabricated on Zeonor©,

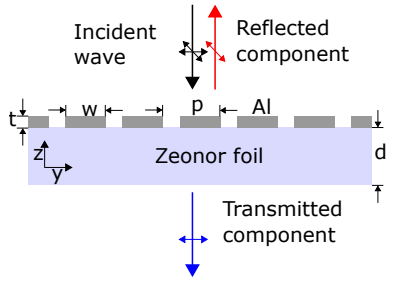

Fig. 1. Schematic diagram of the proposed THz WGP, where d is the Zeonor foil thickness, t the metal thickness, p the wire grid pitch, and w the width of the Al stripes.

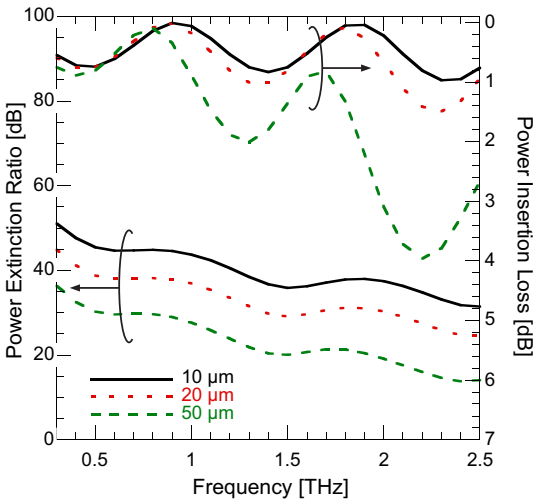

Fig. 2. Numerical investigation of the ER and IL of the THz WGP at normal incidence for a pitch fill factor $F = 70\%$ as a function of the pitch on a 100 µm-thick foil.

a cyclo-olefin polymer substrate with high mechanical flexibility, heat resistance up to 160° C, negligible birefringence, and among the lowest absorption and reflection losses at THz. A systematic numerical parametric study was initially performed, by varying the wire grid period and metal stripe width, in order to identify the structures with a favorable trade-off between IL and achievable ER. Subsequently, the polarizer was fabricated on 100 µm-thick Zeonor© foils. Although standard photolithography techniques have been used for this proof of concept, the polarizer can be fabricated with large metal coaters and/or roll-to-roll patterning techniques over large area at negligible cost [27]. Most importantly, the possibility to bend and conform the fabricated WGP over a rigid surface can open the route for new kinds of integrated and flexible THz devices. Al is here preferred for its lower temperature processing and better compatibility with polymer substrates. The proposed polarizer has an ER between 40 and 45 dB in the 0.3-1 THz range and in excess of 30 dB up to 2.5 THz with an IL below 1 dB. Moreover, due to a refractive index of $\sim$ 1.52 of the polymer foil, the polarizer shows an impedance matching behavior and almost total transmittance at $\sim$ 1 and $\sim$ 2 THz. Finally, we experimentally demonstrate that the performance of the polarizer is preserved even when the latter is bent at a radius of 12.5 mm.

In a WGP the unwanted polarization component $E_{\parallel}$ that is back-reflected is parallel to the metal stripes, while the perpendicular component $E_{\perp}$ is transmitted. Figure 1 shows a

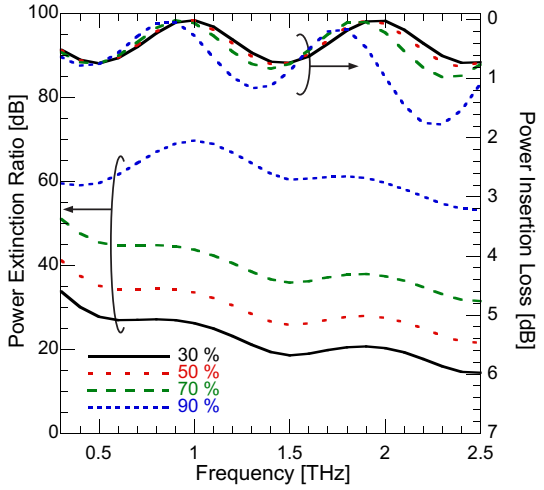

Fig. 3. Numerical investigation of the ER and IL of the THz WGP at normal incidence for $p = 10$ µm pitch on a 100 µm thick-foil as a function of the fill factor.

schematic diagram of the fabricated polarizer where d, t, p, and w are the substrate thickness, the metal thickness, the pitch of the metallic stripe grating, and the width of the metal stripe, respectively. The quality of a polarizer is assessed via the ER

$$\mathrm{ER} = 10\log_{10}\left(T_{\perp}/T_{\parallel}\right) \quad \textbf{(1)}$$

and the IL

$$\mathrm{IL} = -10\log_{10}\left(T_{\perp}/T_{\mathrm{N_2}}\right) \quad \textbf{(2)}$$

where $T_{\perp}$ and $T_{\parallel}$ are the transmitted power coefficients for the field component perpendicular and parallel to the metallic stripes, respectively, while $T_{\mathrm{N_2}}$ is the transmitted power in the absence of the polarizer (all measurements were performed in N_2). An important parameter to be taken into consideration is the skin depth δ of the metal, which for Al is 150 nm and 52 nm at 0.3 THz and 2.5 THz, respectively. The metal thickness must be larger than δ in order to prevent residues of the unwanted polarization component transmitted through the polarizer. We choose $t = 200$ nm, which is thick enough not to notably affect the electromagnetic properties of the polarizer, while it limits the stress on the polymer substrate during fabrication.

A systematic numerical study has been performed and the more significant results are reported in this letter. All simulations were performed by means of the finite-element method, implemented in the commercial solver Comsol Multiphysics©, using periodic boundary conditions at the borders of the unit cell along the grating vector. Al has been modeled as a Drude medium, with plasma frequency $\omega_p = 2.243 \times 10^{16}$ rad/s, and electron decay rate $\gamma = 1.243 \times 10^{14}$ rad/s. The polarizer is illuminated by a plane wave impinging perpendicularly on the structure, as shown in Fig. 1, and the transmission coefficients are calculated for the E_x and E_y components of the electric field.

The key parameters of a WGP are the pitch and the metal width, or equivalently the fill factor F, defined as the ratio w/p. Intuitively, for a given pitch, larger values of ER can be achieved by increasing F, although this comes at the expense of higher IL. The increase of the pitch has a detrimental effect on both ER and IL as the dimensions of the structure become comparable to the operating wavelength. From the complete set of numerical solutions, we focus our attention on achieving high ER, moderate

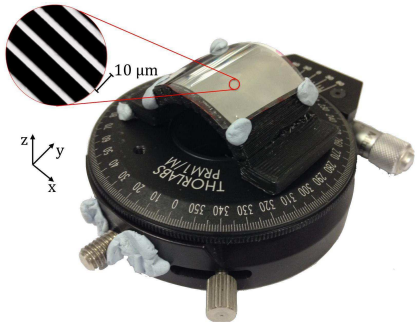

Fig. 4. A flexible THz polarizer on a curved mount, placed on a rotation stage for the THz-TDS experimental setup. The insrt shows a micrograph of the fabricated WGP ($p = 10$ µm and $w = 6.8$ µm) under optical microscope in transmission mode. The black parts are the Al stripes, while the transparent foil appears white.

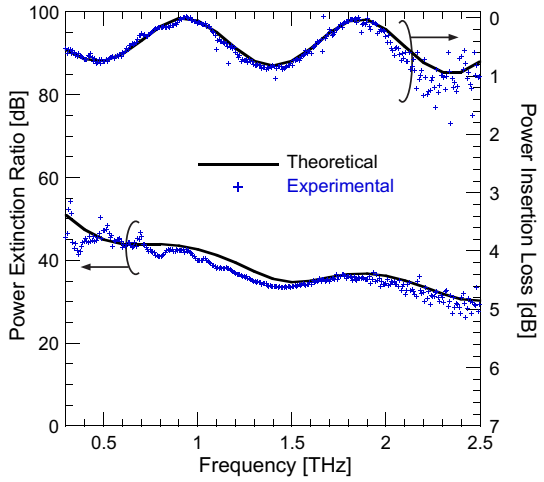

Fig. 5. Comparison of experimental measurements and numerical results of the ER and IL for the THz WGP with $p = 10$ µm and $F = 68\%$ for normal incidence. The scattering of data at higher frequencies is due to the decreasing signal-to-noise ratio of the instrument.

losses and geometries straightforward to fabricate at low cost on large area. Figure 2 shows the power ER and IL for three different grid periods, 10, 20, and 50 µm for the same fill factor of 70%. We limit the design to a 10 µm pitch so that the device is suitable for fabrication also with low cost and large area techniques. The polarizer with 10 µm pitch exhibits the highest ER, with an extremely high value of 50 dB at 0.3 THz and a minimum of 32 dB at 2.5 THz. The ER decreases from the 10 µm case by approximately 6-7 dB and more than 15 dB for $p = 20$ and $p = 50$ µm, respectively. As analytically verified, the IL for $p = 10$ µm is almost exclusively due to the Fabry-Perót (FP) effect in the Zeonor© foil. Hence, almost total transmittance is obtained at ~ 1 THz and ~ 2 THz, while IL remains below 1 dB in the whole spectrum under study. Clearly, similar impedance matching behavior is obtained at other targeted frequencies by tuning d without affecting the structural integrity of the polarizer. The 20 µm period case shows a similar trend with a slightly higher IL, owing to increased reflection of $E_\perp$ due to the metal. For $p = 50$ µm, larger IL values are found, with a maximum of 4 dB. Clearly, the WGP with the smallest period shows the best performance. In Fig. 3 the effect of F in the 30% to 90% range for $p = 10$ µm is presented in detail. Data shows that the higher the F the higher the ER, with a maximum of 70 dB at 1 THz for $F = 90\%$. On the other hand, a large F negatively affects the IL as more extended metallic parts in the structure also increase reflection losses of the $E_\perp$ component.

In the quest for a THz equivalent of the high ER Polaroid, we have fabricated the WGP on a Zeonor© ZF16-100 foil, kindly provided by Zeon Co. The foil is 100 µm thick, highly flexible and conformable. The WGP was fabricated by means of standard photolithography techniques in batches of 2.54×2.54 cm^2 dies. Aluminum was thermally evaporated in high vacuum and the film showed mirror-like quality suitable for visible light. A positive photoresist (Shipley 1813) was spun coated to 1.3 µm thickness, exposed to i-line UV and developed in MIF319 developer. Then, the exposed aluminum is wet-etched in H_3PO_4:H_2O:CH_3COOH:HNO_3=16:2:1:1. The micrograph in the inset in Fig. 4 was taken with a diffraction limited 100x/90 microscope objective, showing no measurable roughness. Finally, dies were cut for mounting in standard 1" rotation stages. However, all fabrication steps are easily extendable to larger area as well as to roll-to-roll processing. The fabricated polarizer (see Fig. 4) was characterized using a Menlo Systems TERA K15 THz-TDS in transmission mode. The frequency dependent dynamic range limits the ER that can be reliably measured to the $F = 70\%$, $p = 10$ µm case. In the inset of Fig. 4, the Al stripes are black and their width is 6.8 µm, while the dielectric foil is white. The pitch of the structure is 10 µm. After processing, the WGP does not show any buckling and maintains its mechanical properties after bending down to curvature with radius 1 cm several times. The source antenna emits a partially polarized THz collimated field with horizontal polarization, which is substantially uniform over an aperture of diameter 25 mm. The frequency-dependent dichroism of the source is not specified by the manufacturer, nor a calibrated polarizer with an ER significantly larger than those fabricated by us was available. Hence, we use two identical polarizers in order to perform a self-referenced measurement [28]. Initially, a first polarizer is set with its easy axis, namely the axis that defines the component of the THz wave that is easily transmitted, at 45° with respect to the polarization of the main component of THz emitted beam. A second polarizer is set perpendicular to the first one and $T_\parallel$ is measured. Then, the second WGP is rotated by 90°, until the maximum detected signal is observed, and $T_\perp$ is recorded. In order to measure the IL, we referenced the transmitted radiation when both the first and the second WGP are into the maximum transmission, *i.e.* with the metal wires perpendicular to the emitted polarization, and thus parallel to each other. Subsequently, the second WGP is removed and the IL are calculated as the ratio between the maximum detected power in the presence of the second WGP and the one measured without it.

Aiming at an accurate comparison with the experimental results, the performance of the WGP was theoretically calculated for the experimentally observed $F = 68\%$. In Fig. 5 we report the comparison between experimental measurements and numerical results of the ER and IL for the WGP with $p = 10$ µm and $F = 68\%$. The experimental data, both in terms of ER and IL show an excellent agreement with the theoretical results. This confirms that the targeted ER is larger than 30 dB, and the IL is lower than 1 dB over the entire frequency range under investigation. Interestingly, the ER is between 40 dB and 45 dB

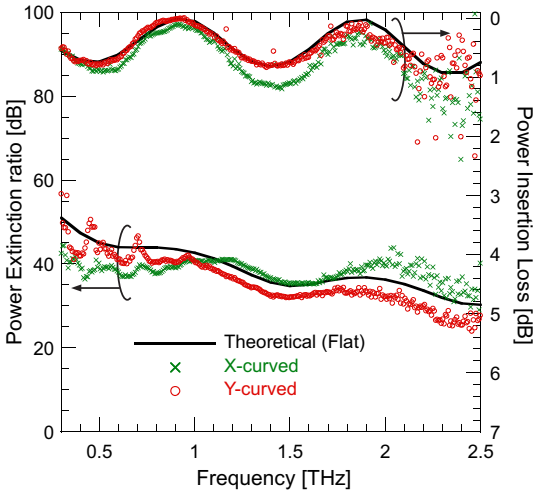

Fig. 6. Experimental investigation of the ER and IL for the THz WGP in two bending configurations ($p = 10$ µm, $F = 68\%$, $R = 12.5$ mm). The theoretical prediction for the flat configuration is included as a reference.

in the 0.3 to 1 THz range, an ER equivalent to state of the art polymer polarizers in the visible range.

Since our THz WGP is fabricated on a flexible foil, we performed, for the first time to the best of our knowledge, the measurement also in two bending configurations using a custom made curved mount with curvature radius $R = 12.5$ mm, as in Fig. 4. We define the "X-curved" configuration as the case for a sample bent along the Al stripes and "Y-curved" when the bent occurs perpendicularly to the grid alignment (reference systems in Fig. 4). The results are illustrated in Fig. 6, where the theoretical lines refer to the flat polarizer studied in Fig. 5. It is shown that, although the bending radius is $R = 12.5$ mm, which significantly distorts the flatness of the polarizer, the performance in both cases is not significantly affected. The ER stays above the target value of 30 dB and reaches values up to 50 dB at the low-frequency edge of the investigated spectrum. The IL are slightly affected, mostly in the X-curved case. This trend is attributed to the change of the effective angle of incidence across the surface of the curved polarizer and it has been corroborated by numerical simulations for different polar and azimuthal angles of incidence. Overall, Figure 4 shows that, thanks to its flexibility, the proposed THz-WGP can also act as a flexible film polarizer, thus expanding its potential as a versatile component in THz setups and applications involving curved surfaces.

To conclude, an Al THz WGP with a pitch of 10 µm and fill factor of 68% was fabricated on a flexible and conformal low-loss Zeonor© dielectric foil. A high experimentally measured ER is between 40 and 45 dB in the 0.3-1 THz range and in excess of 30 dB up to 2.5 THz. Insertion losses are always below 1 dB and vanish at targeted frequencies by tuning the thickness of foil. The performance of the polarizers in bending configurations are only very moderately affected. The experimental results are in excellent agreement with the theoretical study. The ability of the proposed THz-WGP to maintain high performance on curved surfaces paves the way for a new class of flexible and conformal THz devices, such as phase modulators, curved antennas, and radomes. Finally, the polarizer can be fabricated at low cost on large area and can easily be shaped to the desired shape and curvature.

Funding. This work was funded by the Italian Ministry of Foreign Affairs, Directorate General for the Country Promotion and by the Italian Ministry of Education, University and Research (Progetto Premiale THEIA). M. P. acknowledges the support from the Marie Curie Action MC-CIG of the European Union's FP7 Programme under REA grant agreement 630833. The authors would also like to acknowledge the contribution of the COST Action IC1208 (www.ic1208.com).

Acknowledgment. We kindly thank Riccardo Musci from ZEON Co. for valuable support and the supply of materials.

REFERENCES

1. I. F. Akyildiz, J. M. Jornet, and C. Han, Physical Communication **12**, 16–32 (2014).
2. T. Kleine-Ostmann and T. Nagatsuma, J. Infrared Milli. Terahz. Waves **32**, 143–171 (2011).
3. H. B. Liu, Z. Hua, K. Nicholas, C. Yunqing, and X. C. Zhang, Proc. IEEE **95**, 1514–1527 (2007).
4. A. Giles Davies, A. D. Burnett, W. Fan, E. H. Linfield, and J. F. Cunningham, Mater. Today **11**, 18–26 (2008).
5. E. P. J. Parrott, Y. Sun, and E. Pickwell-MacPherson, J. Mol. Struct. **1006**, 66–76 (2011).
6. J.-S. Li, D.-G. Xu, and J.-Q. Yao, Appl. Opt. **49**, 4494–4497 (2010).
7. D. C. Zografopoulos, and R. Beccherelli, Sci. Rep. **5**, 13137 (2015).
8. K. Altmann, M. Reuter, K. Garbat, M. Koch, R. Dąbrowski, and I. Dierking, Opt. Express **21**, 12395–12400 (2013).
9. G. Isić, B. Vasić, D. C. Zografopoulos, R. Beccherelli, and R. Gajić, Phys. Rev. Applied **3**, 064007 (2015).
10. K. Iwaszczuk, A. C. Strikwerda, K. Fan, X. Zhang, R. D. Averitt, and P. U. Jepsen, Opt. Express **20**, 635–643 (2012).
11. M. Shalaby, M. Peccianti, Y. Ozturk, and R. Morandotti, Nature Commun. **4**, 1558 (2013).
12. M. S. Vitiello, G. Scalari, B. Williams, and P. De Natale, Opt. Express **23**, 5167–5182 (2015).
13. Virginia Diodes, Inc. (http://vadiodes.com)
14. M. Y. Glyavin, N. S. Ginzburg, A. L. Goldenberg, G. G. Denisov, A, G. Luchinin, V. N. Manuilov, V. E. Zapevalov, and I. V. Zotova, TST **5**, 67–77 (2012).
15. L. Ren, C. L. Pint, T. Arikawa, K. Takeya, I. Kawayama, M. Tonouchi, R. H. Hauge, and J. Kono, Nano Lett. **12**, 787–790 (2012).
16. C.-F. Hsieh, Y.-C. Lai, R.-P. Pan, and C.-L. Pan, Opt. Lett. **33**, 1174–1176 (2008).
17. J. Zhou, D. R. Chowdhury, R. Zhao, A. K. Azad, H.-T. Chen, C. M. Soukoulis, A. J. Taylor, and J. F. O'hara, Phys. Rev. B **86**, 035448 (2012).
18. K. Shiraishi, S. Oyama, and C. S. Tsai, J. Lightwave Technol. **29**, 670–676 (2011).
19. K. Shiraishi, and K. Muraki, Opt. Express **23**, 16676–16681 (2015).
20. M. Aghadjani, and P. Mazumder, IEEE Trans. Terahertz Sci. Technol. **5**, 556–563 (2015).
21. Microtech Instruments, Inc. (http://www.mtinstruments.com), or Tydex© (http://www.tydexoptics.com)
22. I. Yamada, K. Takano, M. Hangyo, M. Saito, and W. Watanabe, Opt. Lett. **34**, 274–276 (2009).
23. Z. Huang, H. Park, E. P. J. Parrott, H. P. Chan, and E. Pickwell-MacPherson, IEEE Photon. Technol. Lett. **25**, 81–84 (2013).
24. Z. Huang, E. P. J. Parrott, H. Park, H. P. Chan, and E. Pickwell-MacPherson, Opt. Lett. **39**, 793–796 (2014).
25. Y. Kishi, M. Nagai, J. C. Young, K. Takano, M. Hangyo, and T. Suzuki, Appl. Phys. Express **8**, 032201 (2015).
26. K. Takano, H. Yokoyama, A. Ichii, I. Morimoto, and M. Hangyo, Opt. Lett. **36**, 2665–2667 (2011).
27. S. Khan, L. Lorenzelli, and R. S. Dayiha, IEEE Sensors J. **15**, 3164–3185 (2015).
28. F. Yen, C. Yu, H. Park, E. P. J. Parrott, and E. Pickwell-MacPherson, J. Infrared Milli. Terahz. Waves **34**, 489–499 (2013).

REFERENCES

1. I. F. Akyildiz, J. M. Jornet, and C. Han, "Terahertz band: Next frontier for wireless communications," Physical Communication **12**, 16–32 (2014).
2. T. Kleine-Ostmann and T. Nagatsuma, "A review on terahertz communications research," J. Infrared Milli. Terahz. Waves **32**, 143–171 (2011).
3. H. B. Liu, Z. Hua, K. Nicholas, C. Yunqing, and X. C. Zhang, "Terahertz spectroscopy and imaging for defense and security applications," Proc. IEEE **95**, 1514–1527 (2007).
4. A. Giles Davies, A. D. Burnett, W. Fan, E. H. Linfield, and J. F. Cunningham, "Terahertz spectroscopy of explosives and drugs," Mater. Today **11**, 18–26 (2008).
5. E. P. J. Parrott, Y. Sun, and E. Pickwell-MacPherson, "Terahertz spectroscopy - Its future role in medical diagnoses," J. Mol. Struct. **1006**, 66–76 (2011).
6. J.-S. Li, D.-G. Xu, and J.-Q. Yao, "Compact terahertz wave polarizing beam splitter," Appl. Opt. **49**, 4494–4497 (2010).
7. D. C. Zografopoulos, and R. Beccherelli, "Tunable terahertz fishnet metamaterials based on thin nematic liquid crystal layers for fast switching," Sci. Rep. **5**, 13137 (2015).
8. K. Altmann, M. Reuter, K. Garbat, M. Koch, R. Dąbrowski, and I. Dierking, "Polymer stabilized liquid crystal phase shifter for terahertz waves," Opt. Express **21**, 12395–12400 (2013).
9. G. Isić, B. Vasić, D. C. Zografopoulos, R. Beccherelli, and R. Gajić, "Electrically tunable critically coupled terahertz metamaterial absorber based on nematic liquid crystals," Phys. Rev. Applied **3**, 064007 (2015).
10. K. Iwaszczuk, A. C. Strikwerda, K. Fan, X. Zhang, R. D. Averitt, and P. U. Jepsen, "Flexible metamaterial absorbers for stealth applications at terahertz frequencies," Opt. Express **20**, 635–643 (2012).
11. M. Shalaby, M. Peccianti, Y. Ozturk, and R. Morandotti, "A magnetic non-reciprocal isolator for broadband terahertz operation," Nature Commun. **4**, 1558 (2013).
12. M. S. Vitiello, G. Scalari, B. Williams, and P. De Natale, "Quantum cascade lasers: 20 years of challenges," Opt. Express **23**, 5167–5182 (2015).
13. Virginia Diodes, Inc. (http://vadiodes.com)
14. M. Y. Glyavin, N. S. Ginzburg, A. L. Goldenberg, G. G. Denisov, A, G. Luchinin, V. N. Manuilov, V. E. Zapevalov, and I. V. Zotova, "THz gyrotrons - Status and possible optimizations," TST **5**, 67–77 (2012).
15. L. Ren, C. L. Pint, T. Arikawa, K. Takeya, I. Kawayama, M. Tonouchi, R. H. Hauge, and J. Kono, "Broadband terahertz polarizers with ideal performance based on aligned carbon nanotube stacks," Nano Lett. **12**, 787–790 (2012).
16. C.-F. Hsieh, Y.-C. Lai, R.-P. Pan, and C.-L. Pan, "Polarizing terahertz waves with nematic liquid crystals," Opt. Lett. **33**, 1174–1176 (2008).
17. J. Zhou, D. R. Chowdhury, R. Zhao, A. K. Azad, H.-T. Chen, C. M. Soukoulis, A. J. Taylor, and J. F. O'hara, "Terahertz chiral metamaterials with giant and dynamically tunable optical activity," Phys. Rev. B **86**, 035448 (2012).
18. K. Shiraishi, S. Oyama, and C. S. Tsai, "A polarizer using thin metallic-film subwavelength grating for infrared to terahertz region," J. Lightwave Technol. **29**, 670–676 (2011).
19. K. Shiraishi, and K. Muraki, "Metal-film subwavelength-grating polarizer with low insertion losses and high extinction ratios in the terahertz region," Opt. Express **23**, 16676–16681 (2015).
20. M. Aghadjani, and P. Mazumder, "THz polarizer controller based on cylindrical spoof surface plasmon polariton (C-SSPP)," IEEE Trans. Terahertz Sci. Technol. **5**, 556–563 (2015).
21. Microtech Instruments, Inc. (http://www.mtinstruments.com), or Tydex© (http://www.tydexoptics.com)
22. I. Yamada, K. Takano, M. Hangyo, M. Saito, and W. Watanabe, "Terahertz wire-grid polarizers with micrometer-pitch Al gratings," Opt. Lett. **34**, 274–276 (2009).
23. Z. Huang, H. Park, E. P. J. Parrott, H. P. Chan, and E. Pickwell-MacPherson, "Robust thin-film wire-grid THz polarizer fabricated via a low-cost approach," IEEE Photon. Technol. Lett. **25**, 81–84 (2013).
24. Z. Huang, E. P. J. Parrott, H. Park, H. P. Chan, and E. Pickwell-MacPherson, "High extinction ratio and low transmission loss thin-film terahertz polarizer with a tunable bilayer metal wire-grid structure," Opt. Lett. **39**, 793–796 (2014).
25. Y. Kishi, M. Nagai, J. C. Young, K. Takano, M. Hangyo, and T. Suzuki, "Terahertz laminated-structure polarizer with high extinction ratio and transmission power," Appl. Phys. Express **8**, 032201 (2015).
26. K. Takano, H. Yokoyama, A. Ichii, I. Morimoto, and M. Hangyo, "Wire-grid polarizer sheet in the terahertz region fabricated by nanoimprint technology," Opt. Lett. **36**, 2665–2667 (2011).
27. S. Khan, L. Lorenzelli, and R. S. Dayiha, "Technologies for printing sensors and electronics over large flexible substrates: A review," IEEE Sensors J. **15**, 3164–3185 (2015).
28. F. Yen, C. Yu, H. Park, E. P. J. Parrott, and E. Pickwell-MacPherson, "Advances in polarizer technology for terahertz frequency applications," J. Infrared Milli. Terahz. Waves **34**, 489–499 (2013).